International Journal of Trend in Research and Development, Volume 12(3), ISSN: 2394-9333
www.ijtrd.com

Modeling and Experimental Study Forces of Silicon Carbide Ceramics by Longitudinal-Torsional Ultrasonic Grinding

[1]Dengke Yuan and [2]Deyu Zhang,
[1,2]School of Mechanical and Power Engineering, Henan Polytechnic University, Jiaozuo, China.

Abstract: Silicon carbide ceramics are the typical hard and brittle material, and widely used in high-performance components such as high-temperature bearings, high-temperature corrosion-resistant parts, and electronic devices due to their excellent properties, including high hardness, high thermal conductivity, and good wear resistance.In this study, in order to investigate the effects of different process parameters of the grinding forces of silicon carbide ceramics, the longitudinal-torsional ultrasonic grinding force model was established based on the longitudinal-torsional ultrasonic cutting model. Furthermore, the grinding force experimentsof silicon carbide ceramics were conducted by longitudinal-torsional ultrasonic vibration.The experimental results showed that, compared to conventional grinding, the grinding forces were significantly reduced by the introduction of longitudinal-torsional ultrasonic vibration. The normal force was reduced by up to approximately 15.1%, and the tangential force was reduced by up to approximately 14.2%.In addition, it was found that the grinding forces were decreased with the increaseof wheel speed and ultrasonic amplitudeunder longitudinal-torsional ultrasonic vibration, andwere increased with the increase of grinding depth, wheel grit size, and feed rate.

Keywords: *Silicon Carbide Ceramics; Grinding Force; Grinding Process; Longitudinal-Torsional Ultrasonic Vibration*

I. INTRODUCTION

Silicon carbide ceramics are widely applied in fields such as aerospace, mechanical engineering, and semiconductors due to their excellent mechanical properties, outstanding oxidation resistance, high wear resistance, and low friction coefficient[1-2]。At present, precision machining technology is the primary method for grinding silicon carbide ceramics. However, as silicon carbide ceramics are classified as hard and brittle materials, it is difficult to achieve high-quality machining with high efficiency. In particular, various defects and damages, such as degraded layers, surface and subsurface cracks, and surface micro-fractures, are prone to occur during conventional machining processes.These defects and damages not only reduce surface quality and dimensional accuracy but also lower fatigue strength, significantly shortening the service life of the products[3-4]。

To address the challenge of achieving low-damage machining of silicon carbide ceramics, many researchers have introduced ultrasonic machining technology into conventional grinding processes. Zhang et al.[5]developed a grinding force model for elliptical ultrasonic-assisted vibration grinding (UAEVG) of silicon carbide ceramics based on the motion characteristics of abrasive grains, chip deformation mechanisms, and friction laws.Through comparative analysis with conventional grinding (CG) experiments, the results indicated that, compared with conventional grinding, elliptical ultrasonic vibration grinding effectively reduced the grinding forces. The grinding force increased with the rise of undeformed chip thickness but decreased with the increase of wheel speed, and the predicted grinding forces matched well with experimental results, with an average error of approximately 15%.Li et al. [6] established a two-dimensional ultrasonic-assisted grinding force model for silicon carbide considering the material removal mechanism. Through experiments comparing ultrasonic-assisted grinding and conventional grinding, it was demonstrated that the maximum error of the grinding force model was 11.14%. Compared with conventional grinding, the introduction of two-dimensional ultrasonic vibration further reduced the grinding force. Additionally, the grinding force decreased with increasing spindle speed and increased with feed rate, grinding depth, and wheel grit size.Chen et al. [7] investigated the effects of actual amplitude on grinding force and surface quality through comparative experiments of ultrasonic vibration-assisted grinding (UVAFG) and conventional grinding (CG) of silicon carbide ceramics. The results showed that, compared with CG, UVAFG exhibited lower grinding forces and achieved better surface roughness during the grinding of SiC ceramics.Li et al. [8] studied the influence of longitudinal ultrasonic vibration-assisted grinding (UVAG) and conventional grinding (CG) on the grinding forces of silicon carbide ceramics. Experimental results indicated that, compared to CG, UVAG effectively reduced grinding forces and improved surface machining quality. The grinding force increased with grinding depth, feed rate, and ultrasonic amplitude, and decreased with increasing spindle speed.Cao et al. [9] explored the effects of different process parameters on the grinding forces in ultrasonic-assisted internal grinding (UAIG) of silicon carbide ceramics through comparative experiments with conventional grinding. The results demonstrated that, compared with conventional grinding, UAIG reduced the grinding forces. Moreover, the grinding forces increased with feed rate and workpiece rotational speed but decreased with wheel speed, ultrasonic amplitude, and ultrasonic frequency.Currently, research and application of ultrasonic grinding in the field of modern precision machining are receiving increasing attention. Ultrasonic-assisted grinding has become a key focus in studies of material removal mechanisms and surface formation. In particular, longitudinal-torsional ultrasonic vibration-assisted grinding fundamentally alters the motion patterns of abrasive grains, thereby changing the material removal mechanism at its core.

Based on background, this study introduces longitudinal-torsional ultrasonic vibration technology into the ultra-precision machining of high-performance silicon carbide ceramic components. Based on the longitudinal-torsional ultrasonic grinding model of silicon carbide, the motion characteristics during the grinding process are analyzed. Subsequently, a grinding force model for longitudinal-torsional ultrasonic grinding of silicon carbide is established, and experimental investigations on grinding forces are carried out, aiming to provide theoretical support and technical references for the efficient and low-damage machining of hard and brittle materials.

II. ANALYSIS OF MOTION CHARACTERISTICS AND GRINDING FORCE MODELING OF SICBY L-T UAG

A. Analysis of the motion characteristics on L-T UAG

The longitudinal-torsional ultrasonic grinding model is shown in Figure 1. the longitudinal vibration A_b and the torsional vibration A_a in the circumferential direction are superimposed onto the diamond grinding wheel. Meanwhile, the grinding wheel rotates clockwise with the spindle, and the workpiece generates the feed motion v_w relative to the diamond grinding wheel along the axial direction.

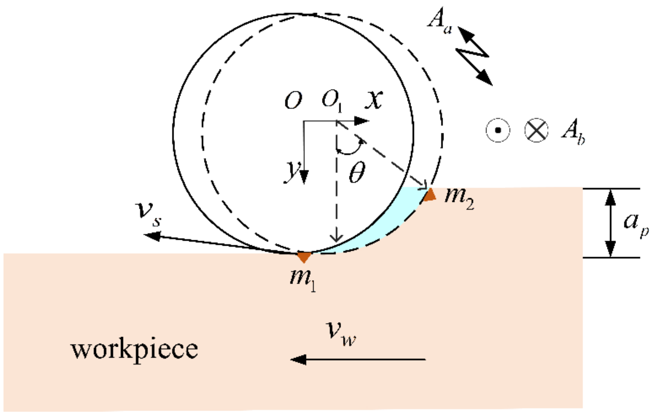

Figure 1. Schematic Diagram of the Longitudinal-Torsional Ultrasonic Grinding Model

According to Figure 1, any abrasive grain begins to engage with the workpiece at point m_1, and separates from the workpiece at point m_2, with a rotation angle of θ. Therefore, the motion trajectory equation of the abrasive grain can be expressed as:

$$\begin{cases} x(t) = R\sin\theta + v_w t \\ y(t) = R\cos\theta \\ z(t) = A_b \sin(2\pi f_b t) \end{cases} \quad (1)$$

where v_w is the feed rate (mm/s) ,R is the radius of the grinding wheel (mm), t is the time during which the abrasive grain engages and disengages with the workpiece, A_b is the longitudinal ultrasonic vibration amplitude (μm), and f_b is the longitudinal ultrasonic vibration frequency(Hz).

According to Figure 2, the grinding speed v_s of the wheel can be obtained by combining its rotational speed v_a and the linear speed v_b of the torsional ultrasonic vibration, which can be expressed by Equation (2).

$$v_s = v_a + v_b = \omega R + 2\pi f_a A_a \cos(2\pi f_a + \varphi) \quad (2)$$

where is w the angular speed of the grinding wheel, w=2πn/60, A_a is the amplitude in the torsional direction μm, f_a is the frequency of torsional vibration Hz, and φ is the phase angle between the axial and circumferential vibrations.

Thus, the cutting arc length of a single abrasive grain under longitudinal-torsional ultrasonic grinding is given by:

$$l_g = \int_0^t v_s dt \quad (3)$$

According to Figure 1, the rotation angle during the engagement and disengagement process of a single abrasive grain can be expressed as:

$$\theta = \frac{l_g}{R} \quad (4)$$

combining Equations (2), (3), and (4), Equation (4) can be rewritten as:

$$\theta = wt + \frac{A_a}{R}\sin\left(2\pi f_a t + \varphi\right) \quad (5)$$

Substitute Equation (5) into Equation (1), the cutting trajectory equation of a single abrasive grain by longitudinal-torsional ultrasonic grinding can be transformed into:

$$\begin{cases} x(t) = R\sin[\omega t + \frac{A_a}{R}\sin(2\pi f_a t + \varphi)] + v_w t \\ y(t) = R\cos[\omega t + \frac{A_a}{R}\sin(2\pi f_a t + \varphi)] \\ z(t) = A_b \sin(2\pi f_b t) \end{cases} \quad (6)$$

When the longitudinal and torsional amplitudes $A_b = A_a = 0$, Equation (6) can be transformed into the cutting trajectory expression of the single abrasive grain in conventional grinding. By differentiating Equation (6) with respect to time, the cutting speed of the single abrasive grain by longitudinal-torsional ultrasonic grinding is obtained as:

$$\begin{cases} v_x = v_w - [\omega R + 2\pi A_a f_a \cos(2\pi f_a + \varphi)]\cos[\omega t + \frac{A_a}{R}\sin(2\pi f_a t + \varphi)] \\ v_y = [\omega R + 2\pi A_a f_a \cos(2\pi f_a + \varphi)]\sin[\omega t + \frac{A_a}{R}\sin(2\pi f_a t + \varphi)] \\ v_z = 2\pi f_b A_b \cos(2\pi f_b t) \end{cases}$$

(7)

In this study, the longitudinal-torsional ratio at the output end of the amplitude modulation rod is 1:1, thus $f_a = f_b = f$. Based on Equations (3) and (7), the cutting arc length of the single abrasive grain by longitudinal-torsional ultrasonic grinding can be expressed as:

$$l_g = \int_0^t \sqrt{v_x^2 + v_y^2 + v_z^2}\, dt =$$

$$\int_0^t \begin{Bmatrix} v_w^2 + 2v_w \cos[\omega t + \frac{A_a}{R}\sin(2\pi ft + \varphi)][\omega R + 2\pi f A_a \cos(2\pi ft + \varphi)] + \\ [\omega R + 2\pi f A_a \cos(2\pi ft + \varphi)]^2 + 4\pi^2 f^2 A_b^2 \cos^2(2\pi ft) \end{Bmatrix}^{1/2} dt$$

(8)

According to Equation (8), when the longitudinal and torsional amplitudes $A_a = A_b = 0$, the equation represents the cutting motion trajectory of a single abrasive grain in conventional grinding. From Equation (8), it can be seen that, due to the introduction of longitudinal-torsional ultrasonic vibration, the cutting arc length of the single abrasive grain per unit time is greater than that in conventional grinding. Furthermore, the cutting arc length increases with the ultrasonic amplitude and frequency, reducing the time the abrasive grain participates in grinding, while improving the surface quality of the silicon carbide workpiece.

B. Establishment of the grinding force model

The Grinding force is an important indicator in the study of the grinding mechanism of silicon carbide materials. Both the surface and subsurface quality during the grinding process are related to the grinding force. To explore the grinding mechanism of of silicon carbide ceramics on longitudinal-torsional ultrasonic grinding, the cutting model for a single abrasive grain under longitudinal-torsional ultrasonic grinding is established, as shown in Figure 2.

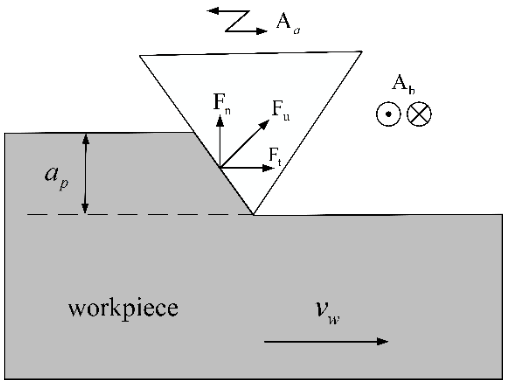

Figure 2: the Cutting Model of the Single Abrasive Grain by L-T UAG

Based on the grinding principle shown in Figure 2, it can be observed that the grinding force of the single abrasive grain is the result of the combined effect of chip deformation force and frictional force. Therefore, the tangential and normal grinding forces of the single abrasive grain by longitudinal-torsional ultrasonic grinding can be expressed as [10].

$$\begin{cases} F_t = F_{tc} + F_{ts} \\ F_n = F_{nc} + F_{ns} \end{cases} \quad (9)$$

where F_t is tangential grinding force of the single abrasive grain, F_n is Normal grinding force of the single abrasive grain, F_{tc} is tangential cutting force of a single abrasive grain, F_{nc} is normal cutting force of a single abrasive grain, F_{ts} is tangential frictional force of a single abrasive grain, F_{ns} is normal frictional force of a single abrasive grain.

In the grinding process, the tangential cutting force F_{tc} and normal cutting force F_{nc} of the single abrasive grain can be expressed as [11]:

$$\begin{cases} F_{tc} = \dfrac{\pi}{4\tan\theta} F_p \cdot A_u \\ F_{nc} = F_p A_u \end{cases} \quad (10)$$

where A_u is Cutting chip cross-sectional area of the single abrasive grain, F_p is Radial grinding force per unitchip cross-sectional area (N), $F_p = F_0 a_p{}^{2r} \tan^r \theta$ (-0.95 < r < -0.5), F_0 is Unit grinding force constant, θ is Abrasive grain rake angle.

To facilitate the analysis of the chip cross-sectional area, the removal cross-sectional area of the abrasive grain is simplified as an isosceles triangle. The size of the chip cross-sectional area directly affects the amount of material removed by the abrasive grain per unit time. The material removal rate per unit time can be expressed as [12]:

$$W = C \cdot b \cdot v_s \cdot V_u \quad (11)$$

Where W is Material removal rate per unit time, b is Grinding width, v_s is Grinding speed, V_u is Grinding removal depth, C is Number of effective abrasive grains per unit grinding area of the wheel.

During the grinding process, the material removal volume (material removal rate) per unit time for the single abrasive grain can be expressed as:

$$MRR = a_p v_w b \quad (12)$$

where MRR is Material removal rate, a_p is Grinding depth, v_w is Feed rate. There is a balance relationship between the amount of chips removed per unit time and the material removal rate. By combining Equations (11) and (12), the material removal amount of the single abrasive grain can be obtained as:

$$V_u = \frac{a_p v_w}{C v_s} \quad (13)$$

The relationship between the material removal amount of the single abrasive grain and the chip cross-sectional area can be expressed as:

$$V_u = A_u l_g \quad (14)$$

By substituting Equation (13) into Equation (14), the chip cross-sectional area of a single abrasive grain can be obtained as:

$$A_u = \frac{a_p v_w}{C v_s l_g} \quad (15)$$

combining Equations (8), (10), and (15), the tangential cutting force and normal cutting force of the single abrasive grain by L-T UAG can be obtained as:

$$\begin{cases} F_{tc} = \dfrac{\pi F_0 a_p{}^{2r+1} v_w \tan^{r-1}\theta}{4C v_s \cdot \int_0^t \sqrt{\begin{array}{l} v_w^2 + 2v_w \cos[wt + \frac{A_a}{R}\sin(2\pi ft+\varphi)][wR + 2\pi f A_a \cos(2\pi ft+\varphi)] + \\ [wR + 2\pi f A_a \cos(2\pi ft+\varphi)]^2 + 4\pi^2 f^2 A_b^2 \cos^2(2\pi ft) \end{array}}} \\ F_{nc} = \dfrac{F_0 a_p{}^{2r+1} \tan^r\theta}{C v_s \cdot \int_0^t \sqrt{\begin{array}{l} v_w^2 + 2v_w \cos[\omega t + \frac{A_a}{R}\sin(2\pi ft+\varphi)][wR + 2\pi f A_a \cos(2\pi ft+\varphi)] + \\ [wR + 2\pi f A_a \cos(2\pi ft+\varphi)]^2 + 4\pi^2 f^2 A_b^2 \cos^2(2\pi ft) \end{array}}} \end{cases} \quad (16)$$

when the single abrasive grain grinds the workpiece surface, The normal friction force and tangential friction force generated can be expressed as [13]:

$$\begin{cases} F_{ts} = \mu \tau_0 \bar{p} \\ F_{ns} = \tau_0 \bar{p} \end{cases} \quad (17)$$

where μ is the coefficient of friction between the workpiece and the abrasive grain, τ_0 is the tip area of the abrasive grain, $\bar{p}$ the average contact pressure between the workpiece and the tip region of the abrasive grain, $\bar{p} = 4v_w p_0 / d_e v_s$, p_0 is proportional constant.

Combining Equations (9), (16), and (17), the normal grinding force and tangential grinding force of a single abrasive grain by L-T UAG can be obtained as:

$$\begin{cases} F_n = \dfrac{4\mu\tau_0 p_0 v_w}{d_e v_s} + \dfrac{F_0 a_p^{2r+1} \tan^r \theta}{Cv_s \cdot \int_0^t \sqrt{\begin{aligned} & v_w^2 + 2v_w \cos[wt + \frac{A_a}{R}\sin(2\pi ft + \varphi)][wR + 2\pi fA_a \cos(2\pi ft+\varphi)] + \\ & [wR + 2\pi fA_a \cos(2\pi ft + \varphi)]^2 + 4\pi^2 f^2 A_b^2 \cos^2(2\pi ft) \end{aligned}}\, dt} \\ F_t = \dfrac{4\tau_0 p_0 v_w}{d_e v_s} + \dfrac{\pi F_0 a_p^{2r+1} v_w \tan^{r-1} \theta}{4Cv_s \cdot \int_0^t \sqrt{\begin{aligned} & v_w^2 + 2v_w \cos[wt + \frac{A_a}{R}\sin(2\pi ft + \varphi)][wR + 2\pi fA_a \cos(2\pi ft+\varphi)] + \\ & [wR + 2\pi fA_a \cos(2\pi ft + \varphi)]^2 + 4\pi^2 f^2 A_b^2 \cos^2(2\pi ft) \end{aligned}}\, dt} \end{cases} \quad (18)$$

During the contact process between diamond abrasive grains and the grinding zone, variations in the protrusion heights of the abrasive grains on the wheel cause dynamic fluctuations in the number of effective abrasive grains participating in cutting within the grinding zone. The dynamic number of abrasive grains in the grinding zone N_d can be expressed as:

$$N_d = Cbtv_s \quad (19)$$

where b is the grinding width, and t is the engagement time of the single abrasive grain.

combining Equations (18) and (19), the normal grinding force and tangential grinding force by L-T UAG can be obtained as follows:

$$\begin{cases} F_N = N_d F_n = \dfrac{4C\mu\tau_0 p_0 v_w bt}{d_e} + \dfrac{4F_0 b a_p^{2r+2} \tan^r \theta t}{\int_0^t \sqrt{\begin{aligned} & v_w^2 + 2v_w \cos[wt + \frac{A_a}{R}\sin(2\pi ft + \varphi)][wR + 2\pi fA_a \cos(2\pi ft+\varphi)] + \\ & [wR + 2\pi fA_a \cos(2\pi ft + \varphi)]^2 + 4\pi^2 f^2 A_b^2 \cos^2(2\pi ft) \end{aligned}}\, dt} \\ F_T = N_d F_t = \dfrac{4C\tau_0 p_0 v_w bt}{d_e} + \dfrac{\pi F_0 b a_p^{2r+1} v_w \tan^{r-1} \theta t}{4 \cdot \int_0^t \sqrt{\begin{aligned} & v_w^2 + 2v_w \cos[wt + \frac{A_a}{R}\sin(2\pi ft + \varphi)][wR + 2\pi fA_a \cos(2\pi ft+\varphi)] + \\ & [wR + 2\pi fA_a \cos(2\pi ft + \varphi)]^2 + 4\pi^2 f^2 A_b^2 \cos^2(2\pi ft) \end{aligned}}\, dt} \end{cases} \quad (20)$$

According to the above grinding force model, compared with conventional grinding, the grinding force was reduced because ofthe introduction of longitudinal-torsional ultrasonic vibration. Meanwhile, the wheel speed n, grinding depth, feed rate, and ultrasonic amplitudes and play key roles in determining the magnitude of the grinding forces. During the longitudinal-torsional ultrasonic vibration grinding process, both the normal and tangential grinding forces were decreased with increasing wheel speed and ultrasonic amplitudes, and were increased with increasing grinding depth and feed rate.

III. EXPERIMENTAL STUDY ON THE GRINDING FORCES OF SICBYL-T UAG

To further verify the accuracy of the grinding force model, this section conducts single-factor longitudinal-torsional ultrasonic vibration grinding experiments on silicon carbide ceramics. The effects of machining parameters on the normal and tangential grinding forces are investigated and compared with those under conventional grinding.

A. Experimental materials and tools

The workpiece used in the experiment was reaction-bonded silicon carbide (RB-SiC) ceramic, produced by Fuzhou Zhonghuan Precision Technology, The dimensions of the workpiece were 15 mm×10 mm×5 mm, and its main material properties are listed in Table1.the grinding wheels were resin-bonded diamond wheels with grit sizes of#100, #200, and#300, and grinding wheel concentration is 100%.the dimensions of the grinding wheels were 15 mm × 10 mm× 8mm × 6 mm, the diamond grinding wheels and the RB-SiC ceramic workpiece are shown in Figure 3.

Table 1: Main performance parameters of the workpiece

Material	Density (kg/m^3)	Hardness (GPa)	Fracture toughness ($MPa{\cdot}m^{1/2}$)	Elastic modulus (GPa)	Poisson's ratio
SiC	3560	33	5	410	0.14

(a) Diamond Grinding Wheel

(b) Silicon Carbide Workpiece

Fig.3 Diamond grinding wheel and SiC

B. Build of the experimental platform

The longitudinal-torsional ultrasonic vibration grinding experimental platform built for this study is shown in Figure 4. As seen in Figure 4, The experimental platform is consisted of the three-axis vertical machining center and a longitudinal-torsional ultrasonic vibration system. The machining center used is manufactured by Shenyang Machine (VMC850E), with relevant performance parameters listed in Table 2. The longitudinal-torsional ultrasonic vibration system is comprised of the 35 kHz ultrasonic generator, wireless transmission system, piezoelectric ceramic transducer, longitudinal-torsional composite vibration amplitude rod, and a BT40 tool holder.

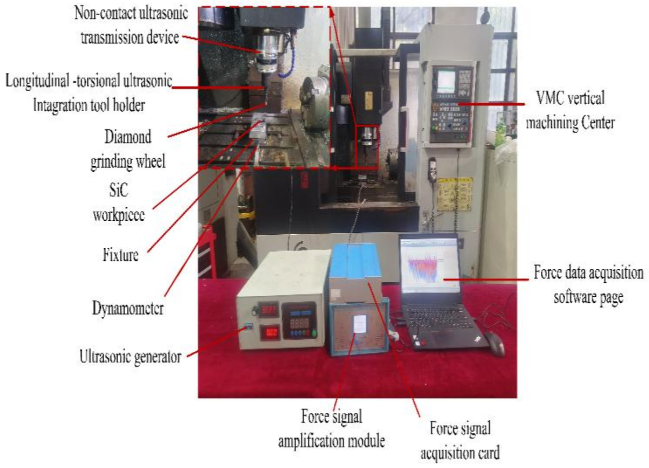

Fig.4 Experimental platform of L-T UAG

Tab. 2 Performance parameters of the three-axis Vertical Machining Center (VMC850E).

Project	X/Y/Z axis travel	Spindle power	Speed range	Max output torque	Positionin g accuracy
paramet er	850/500/540mn	7.5/11kw	50~8000r/mir	35.8N · m	0.005mm

Before the experiment, the displacement sensor was used to measure the amplitude of the longitudinal-torsional ultrasonic system. Since measuring the torsional amplitude is more challenging,the longitudinal vibration amplitude was measured, and the torsional vibration amplitude was calculated using the longitudinal-torsional ratio (1:1). The amplitude testing setup is shown in Figure 5.

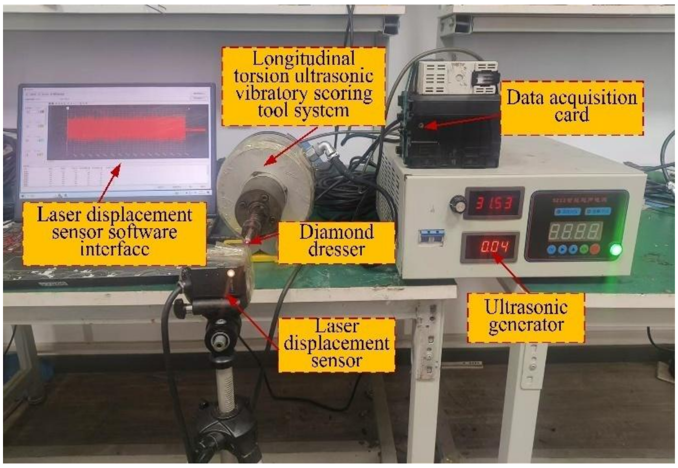

Fig. 5 Ultrasonic Vibration Amplitude Testing Site

During the testing process, the laser displacement sensor's cursor is aligned with the diamond grinding wheel's end face. When the cursor displays green, the vibration amplitude can be measured. Multiple measurements are taken, and the average value is considered as the final measurement result. The measurement results show that the maximum amplitude is 6.42, which meets the experimental requirements.

C. Design of Grinding Experiment Scheme

Before the grinding experiment, the end of the grinding wheel was fixed to the longitudinal-torsional ultrasonic tool holder using a spring collet. The workpiece was positioned and clamped onto the machine tool table using a fixture. Side dry grinding was employed. To eliminate the influence of workpiece dimensional tolerances on the experimental results, the surface to be machined was leveled prior to the test. When the grinding force signal became stable without significant fluctuations, the machining condition was considered satisfactory. During the experiment, the dynamometer (Kistler 9257B) was used to continuously collect real-time force signal variations.

To investigate the influence of different process parameters on the grinding forces of silicon carbide during longitudinal-torsional ultrasonic vibration diamond grinding, single-factor grinding experiments were designed. The experimental parameters are listed in Table 3.

Tab. 3 Single-factor experimental parameters

Number	Grit size	Grinding speed	Grinding depth	Feed rate	Ultrasonic amplitude
D1	#100	3500	8	200	4
D2	#200	3500	8	200	4
D3	#300	3500	8	200	4
D4	#200	1500	8	200	4
D5	#200	2500	8	200	4
D6	#200	3500	8	200	4
D7	#200	4500	8	200	4
D8	#200	3500	4	200	4
D9	#200	3500	8	200	4
D10	#200	3500	12	200	4
D11	#200	3500	16	200	4
D12	#200	3500	8	1 00	4
D13	#200	3500	8	150	4
D14	#200	3500	8	200	4
D15	#200	3500	8	250	4
D16	#200	3500	8	200	0
D17	#200	3500	8	200	2
D18	#200	3500	8	200	4
D19	#200	3500	8	200	6

D. Experimental results and analysis of grinding forces

The magnitude of the grinding force is an important indicator of grinding quality. The normal grinding force is a major cause of surface and subsurface cracks, while the tangential grinding force directly affects machining efficiency. Due to the relatively small magnitude of the radial grinding force, it is neglected in this study. To ensure the accuracy of the experimental results, each group of grinding tests was repeated three times, and the average value was taken as the final result. The detailed experimental results are shown in Table 4.

Tab. 4 Grinding force experimental data

Number	Normal Force (CG)N	Tangential Force (CG) N	Normal Force (UG) N	Tangential Force (UG) N
D1	14.82	6.01	12.12	4.88

D2	12.41	4.86	9.79	3.87
D3	10.59	3.66	8.48	2.63
D4	14.94	6.83	13.09	5.52
D5	12.74	5.71	11.06	4.44
D6	11.46	4.46	9.49	3.87
D7	9.96	3.78	8.57	2.75
D8	8.45	2.99	7.03	2.17
D9	9.39	3.36	8.69	2.94
D10	11.26	4.12	9.79	3.87
D11	13.21	5.62	12.64	4.95
D12	8.52	3.19	7.44	2.37
D13	10.14	3.86	8.26	3.01
D14	12.36	4.42	9.79	3.87
D15	14.56	5.67	12.01	4.93
D16	14.33	6.62	12.45	5.38
D17	12.29	5.52	10.69	4.61
D18	11.14	4.47	9.79	3.87
D19	9.65	4.48	8.24	3.31

2.4.1 Effect of grinding wheelgrit size on grinding force

The size of the grinding wheel grit directly affects the grinding force between the abrasive particles and the grinding area within a unit time. As the grit size decreases, the number of abrasive particles engaging in the grinding area increases, leading to improved surface quality of the grinding region. Figure 6 illustrates the influence of different grinding wheel grits on the grinding force.

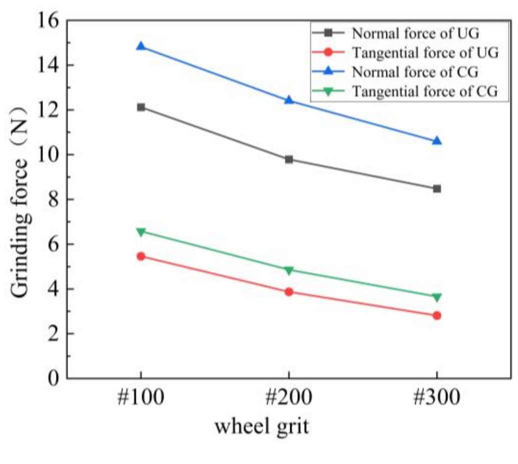

Fig. 6 The Effect of wheel grit size on grinding force.

As shown in Figure 6, both the normal grinding force and the tangential grinding force decrease as the wheel grit size decreases. This is because, as the wheel grit size decreases, the size of the abrasive grains becomes smaller, which reduces the maximum undeformed chip thickness during the silicon carbide removal process. The volume of material removed by a single abrasive grain decreases, and the area involved in the cutting process of the grain also decreases. The material's resistance to deformation is reduced. With the same grinding contact area, smaller abrasive grains result in fewer grains per unit area, leading to a reduction in grinding resistance and, therefore, a decrease in the overall grinding force. Additionally, as shown in Figure 6, compared to conventional grinding, the grinding force in longitudinal-torsional ultrasonic grinding is lower. This is because, under the effect of ultrasonic vibration, the abrasive grains intermittently contact the grinding area, reducing the resistance between the grains and the grinding area within the same unit of time, improving the sharpness of the abrasive grains, and preventing the increase in grinding force caused by grain dulling. Ultrasonic vibration not only increases the contact arc length of the grinding area but also reduces the maximum undeformed chip thickness during silicon carbide removal, thus lowering the grinding force generated by the material's resistance to deformation. Therefore, appropriately reducing the wheel grit size can reduce the grinding force.

2.4.2 The Effect of Wheel Speed on Grinding Force.

Figure 7 shows the effect of wheel speed on the grinding force of silicon carbide ceramics during conventional grinding and longitudinal-torsional ultrasonic grinding under the parameters of wheel grit size#200, grinding deptha_p=8μm, feed rate $v_w = 100$mm/min , and ultrasonic amplitude A=4μm .From the figure, it can be seen that both the normal grinding force and the tangential grinding force decrease with the increase of wheel speed. This is because an increase in wheel speed leads to the higher grinding velocity, which raises the shear rate of silicon carbide per unit time and reduces the maximum undeformed chip thickness, thereby lowering the grinding force. In addition, the grinding force under ultrasonic grinding is lower than that under conventional grinding. This is because ultrasonic vibration causes the abrasive grains to intermittently contact the grinding area, increasing the contact arc length, enhancing the strain rate and dynamic fracture toughness of the silicon carbide material. Meanwhile, ultrasonic vibration reduces abrasive grain wear, and broken grains adhered to the wheel surface are more easily removed under vibration, improving the self-sharpening ability of the diamond abrasives, thus leading to a reduction in grinding force. As the wheel speed continues to increase, the difference between ultrasonic grinding force and conventional grinding force becomes smaller because, at higher wheel speeds, the separation effect of the torsional ultrasonic vibration weakens, making the ultrasonic effect less significant.

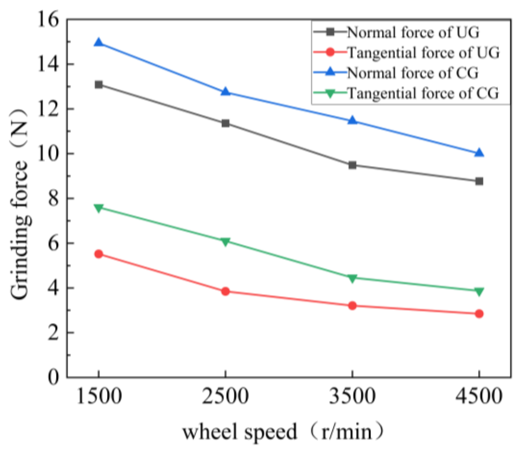

Fig. 7 The effect of wheel speed on grinding force

2.4.3 The effect ofgrinding depth on grinding force.

Figure 8 shows the effect of different grinding depths on the grinding force of silicon carbide ceramics under the parameters of wheel grit size #200, wheel speed $n = 3500$r/min , feed rate $v_w = 100$mm/min , and ultrasonic amplitude A=4μm .

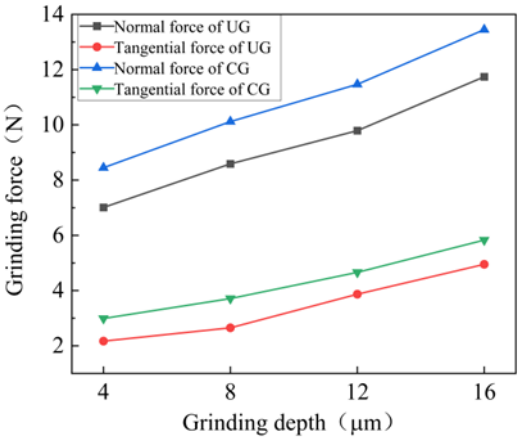

Fig. 8 The effect of grinding depth on grinding force.

According to Figure 8, the grinding force increases with the increase of grinding depth. Under the same processing conditions, the grinding force in ultrasonic grinding is lower than that in conventional grinding. Compared to conventional grinding, the normal force is reduced by up to approximately 15.1%, and the tangential force is reduced by up to approximately 14.2%. This is because, during ultrasonic grinding, the cutting cross-sectional area engaged by the abrasive grains is smaller than that in conventional grinding, resulting in fewer abrasive grains participating per unit area, and the maximum undeformed chip thickness during the silicon carbide removal process is also smaller. However, as the grinding depth continues to increase, the grinding force in both processing methods increases significantly. This is because a greater grinding depth leads to increased friction between the abrasive grains and the material in the contact area, higher grinding temperatures, and a higher likelihood of wheel clogging, all of which contribute to an increase in grinding force.

2.4.4 The effect of feedrate on grinding force.

Figure 9 shows the effect of different feed rates on the grinding force of silicon carbide ceramics under conventional grinding and longitudinal-torsional ultrasonic grinding, with the parameters of wheel grit size #200, wheel speed $n = 3500 \text{r/min}$, grinding deptha_p=8μm,, and ultrasonic amplitudeA=4μm. As seen in Figure 9, the grinding force under both grinding methods increases with the increase in feed rate. However, when the feed rate reaches 250 mm/min, the increasing trend slows down. This is because as the feed rate increases, the maximum undeformed chip thickness for each abrasive grain also increases, resulting in a greater volume of material removal from the silicon carbide workpiece. Consequently, the shear force and frictional resistance between the abrasive grains and the grinding area increase, leading to a rise in grinding force.

Under the same processing conditions, the grinding force in longitudinal-torsional ultrasonic grinding is lower than that in conventional grinding. This is attributed to the high-frequency contact-separation effect induced by longitudinal-torsional ultrasonic vibration, causing the diamond abrasive grains to intermittently contact the silicon carbide grinding area. This results in chips fracturing rapidly under cyclic high stress. The ultrasonic superposition effect also promotes brittle fracture in the silicon carbide material, with the generated cracks continuously propagating and intersecting, causing the material to break off in chunks, thereby reducing the grinding force.

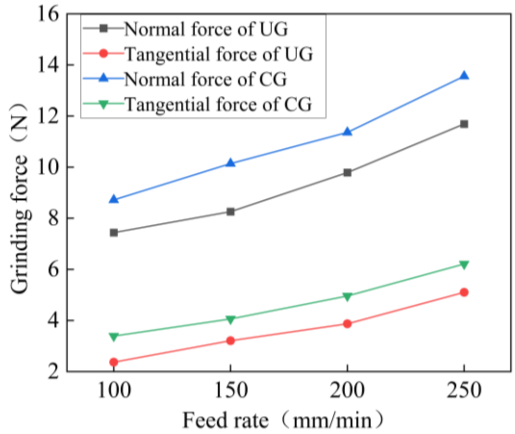

Fig. 9 The effect of feed rate on grinding force.

2.4.5 The effect of ultrasonicamplitude on grinding force.

Figure 10 shows the effect of different ultrasonic amplitudes on the grinding force of silicon carbide ceramics under longitudinal-torsional ultrasonic grinding, with the parameters of wheel grit size #200, wheel speed n=3500r/min , grinding depth $a_p = 8\mu\text{m}$, and feed rate $v_w = 100\text{mm/min}$.

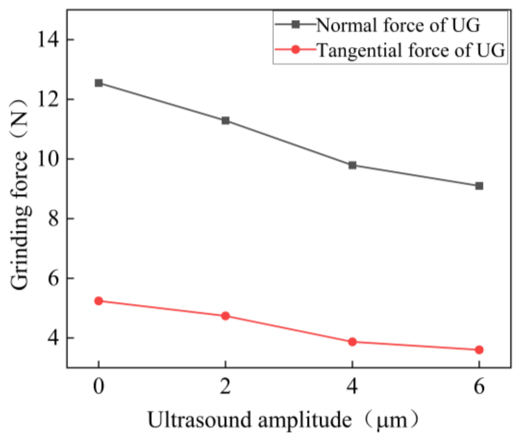

Fig. 10 The effect of ultrasonic amplitude on grinding force.

As shown in Figure 10, the increase in ultrasonic amplitude reduces the grinding force. This is because high-frequency ultrasonic vibration accelerates the contact frequency between the abrasive grains and the workpiece, shortening the contact time between them. The removal efficiency of silicon carbide ceramics improves, making it easier for chips to be expelled from the processing area, and the grinding heat is quickly dissipated. The superimposed effect of the abrasive grain trajectories increases the strain rate and dynamic fracture toughness of silicon carbide, thereby expanding its plastic deformation region. However, as the amplitude continues to increase, when the vibration amplitude reaches 6 μm , the reduction in grinding force becomes less pronounced. This is because when the ultrasonic amplitude is too large, the instantaneous cutting thickness for abrasive grains is increased, and the impact of the grains is enhanced, which may lead to surface hardening of the silicon carbide, thus weakening the ultrasonic effect.

CONCLUSION

(1) Based on the analysis of the longitudinal-torsional ultrasonic grinding motion characteristics, the kinematic trajectory of the single abrasive grain was established by

longitudinal-torsional ultrasonic grinding. The simulation analysis of the motion trajectories of multiple abrasive grains was conducted to analyze the material processing mechanismunder both conventional grinding and longitudinal-torsional ultrasonic grinding. The results show that the introduction of ultrasonic vibration causes the cutting trajectory of the single abrasive grain to follow a spiral curve, the cutting arc length of a single abrasive grain was increased, the mutual interference between multiple abrasive grains wasintensified, which in turn the material removal from the grinding surface wasenhanced and the surface quality was improved

(2) Based on the longitudinal-torsional ultrasonic cutting model, the longitudinal-torsional ultrasonic grinding force model for silicon carbide ceramics was established, and longitudinal-torsional ultrasonic grinding force experiments for silicon carbide were conducted. Theoretical and experimental results indicate that, compared to conventional grinding, the introduction of longitudinal-torsional ultrasonic vibration effectively reduces the grinding force. Additionally, the grinding forcewas decreased withincrese the wheel speed and ultrasonic amplitude, while was increasedwith increas grinding depth, wheel grit size, and feed rate.

References

[1] Ye Z, Wen X, Wan W, et al. Precision Grinding Technology of Silicon Carbide (SiC) Ceramics by Longitudinal Torsional Ultrasonic Vibrations[J]. Materials (Basel), 2023,16(16):5572.

[2] Chen Y, Su H, He J, et al. The Effect of Torsional Vibration in Longitudinal－Torsional Coupled Ultrasonic Vibration-Assisted Grinding of Silicon Carbide Ceramics: Materials[Z]. 2021: 14.

[3] Li C, Wang K, Zakharov O, et al. Damage evolution mechanism and low-damage grinding technology of silicon carbide ceramics[J]. International Journal of Extreme Manufacturing, 2025,7(2):22015.

[4] Rao X, Zhang F, Luo X, et al. Material removal mode and friction behaviour of RB-SiC ceramics during scratching at elevated temperatures[J]. Journal of the European Ceramic Society, 2019,39(13):3534-3545.

[5] Zhang K, Dai C, Yin Z, et al. Modeling and prediction on grinding force in ultrasonic assisted elliptical vibration grinding (UAEVG) of SiC ceramics using single diamond grain[J]. Journal of Manufacturing Processes, 2024,131:2244-2254.

[6] Li H, Chen T, Duan Z, et al. A grinding force model in two-dimensional ultrasonic-assisted grinding of silicon carbide[J]. Journal of Materials Processing Technology, 2022,304:117568.

[7] Chen Y, Su H, Qian N, et al. Ultrasonic vibration-assisted grinding of silicon carbide ceramics based on actual amplitude measurement: Grinding force and surface quality[J]. Ceramics International, 2021,47(11):15433-15441.

[8] Li C, Zhang F, Meng B, et al. Material removal mechanism and grinding force modelling of ultrasonic vibration assisted grinding for SiC ceramics[J]. Ceramics International, 2017,43(3):2981-2993.

[9] Cao J, Wu Y, Li J, et al. A grinding force model for ultrasonic assisted internal grinding (UAIG) of SiC ceramics[J]. International Journal of Advanced Manufacturing Technology, 2015,81(5-8):875-885.

[10] Malkin S, Guo C. Grinding technology: theory and application of machining with abrasives[M]. Industrial Press Inc., 2008.

[11] Lichun L, Jizai F, Peklenik J. A study of grinding force mathematical model[J]. CIRP Annals, 1980,29(1):245-249.

[12] Wu Z, Zhang L. Analytical grinding force prediction with random abrasive grains of grinding wheels[J]. International Journal of Mechanical Sciences, 2023,250:108310.

[13] Azarhoushang B. Abrasive Machining Processes[J]. Tribology and Fundamentals of Abrasive Machining Processes, 2021